Chemiluminescence of Spherically Expanding Methane-Air Flames Doped with DMMP

Mattias A. Turner, Pradeep Parajuli, Waruna D. Kulatilaka, and Eric L. Petersen
J. Mike Walker '66 Department of Mechanical Engineering, Texas A&M University
College Station, Texas 77843 USA

1 Introduction

The study of the combustion of phosphorus-containing compounds is relevant for two different applications: for use as fire suppressants and as surrogates of sarin ($C_4H_{10}FO_2P$). As fire suppressants, organophosphorus compounds (OPCs) such as DIMP ($C_7H_{17}O_3P$), DMMP ($C_3H_9O_3P$), TEP ($C_6H_{15}O_4P$), and others show promise as replacements for substances such as halons [1] that have been phased out by the Montreal Protocol. Recent work in the authors' laboratory has shown that H_2- and CH_4-air flames doped with small (0.1-0.3 vol%) OPC concentrations exhibit decreased laminar flame speeds relative to the parent mixtures by up to 30% [1, 2], although numerical work by Babushok et al. [3] indicated that DMMP addition increases the flame speed of lean hydrocarbon mixtures due to increased hydrocarbon moiety. For ignition delay time, the effect of OPC addition varies with the parent fuel molecule [2, 4].

Incineration of sarin has been proposed as a method of its destruction, and due to obvious safety considerations, experimental investigations rely on surrogates like OPCs. Identifying chemiluminescent markers of OPC combustion, and therefore sarin combustion, can provide a method of verifying the successful destruction of sarin. Various OPCs have been investigated for their similarities to sarin in their molecular structure and in their mechanism of thermal decomposition [5]. Kinetic modeling by Glaude et al. [6] has indicated that of DMMP, TMP, and DIMP, the latter most closely matches the incineration behavior of sarin. Twarowski [7-9] detailed the inhibition mechanism of P-containing fire suppressants, pointing out that the key P-containing species HOPO, $HOPO_2$, and PO_2 act to redirect the key combustion radicals H and OH. The electronically excited states of these P-containing intermediates can provide chemiluminescence markers that help identify combustion of OPCs, but an adequate phosphorus chemiluminescence combustion diagnostic has escaped investigators thus far.

Chemiluminescence from phosphorus oxidation reactions has been observed for centuries, but only in the past few decades has there been any progress on identifying the responsible species. Davies and Thrush [10] first attributed the visible continuum to PO_2* by analogy to the well-studied NO_2* chemiluminescence continuum. Flash photolysis experiments by Verma and McCarthy [11] concluded that the observed spectrum originated from PO_2*. Fraser and Stedman [12] also suggested that the visible continuum was due to PO_2* because their low-pressure experiments precluded the formation of an excimer. Harris, Chou, and Cool [13] observed a similar continuum of chemiluminescence from reactions of phosphine (PH_3) and nitrous oxide (N_2O), and attributed the continuum to emission from an excited molecule containing only phosphorus and oxygen, most likely PO_2*. Around the same time,

Correspondence to: mattias.turner@tamu.edu

Hamilton and Murrells [14, 15], using the reaction O + PH_3, effectively established PO_2* as the source of the continuum of chemiluminescence starting near 330 nm and extending into the infrared (IR).

All of these previous investigations of chemiluminescence of phosphorus oxidation were conducted without the presence of carbon-containing compounds. The objective of this study was to identify effects of OPC addition on the chemiluminescent spectra of hydrocarbon flames and determine if a unique chemiluminescence marker could be linked to a phosphorus intermediate. The study comprised spherically expanding flame tests, conducted for methane-air and DMMP-methane-air mixtures. The paper describes the experimental facilities, optical diagnostics, and procedural methodologies used to make measurements of chemiluminescence spectra from 200-800 nm in Section 2. Results are presented in Section 3, comparing spectra of neat mixtures and OPC-doped mixtures side-by-side. The effects of OPC addition on the spectra are discussed as the results are presented.

2 Experimental Procedure and Data Analysis

Emission spectra were collected using a fiber-coupled spectrometer (Princeton Instruments, Model: IsoPlane 160) fitted with an intensified charge-coupled device (ICCD) camera (Princeton Instruments, Model: PIMax4). The vertical entrance slit width was opened to 150 μm. Gratings with 300 lines/mm and 1200 lines/mm were used for low- and high-resolution data recording, respectively. The 300-lines/mm grating provided a spectral resolution of approximately 0.204 nm/pixel, while that of the 1200-lines/mm grating was 0.049 nm/pixel. Of course, this four-fold improvement in resolution was offset by approximately a four-fold decrease in the viewable wavelength range per spectrum. The combined spectrometer-camera system is sensitive over a wavelength region from 200–850 nm; however, the measurable wavelength range per spectrum is restricted to approximately 200 nm for low-resolution tests and approximately 50 nm for high-resolution tests. For the low-resolution tests, this required that three experiments be conducted at each ϕ to capture emission for the full 200–800 nm range: first at 300±100 nm, then at 500±100 nm, and finally at 700±100 nm. The high-resolution tests were conducted at 300±25 nm and 430±25 nm to obtain detailed spectra of OH* and CH* emission, respectively.

Spherically expanding flame experiments were conducted using the Turbulent Flame Speed Vessel (TFSV) at Texas A&M University. The TSFV is a constant-volume, stainless steel chamber of approximately 34 L of internal volume and has four optical ports of 12.7 cm in diameter. The chamber is equipped with stirring fans and internal resistance heaters. More details of the TFSV are given by Morones et al. [16]. A collimating lens, positioned at the center of one of the windows of the chamber and coupled to an optical fiber, captured emission from the flame and delivered it to the spectrometer. Simultaneously, to monitor flame propagation and verify the timing of the spectrometer recording, a schlieren imaging system comprised of a mercury arc lamp and a Photron Fastcam SA1.1 was used. The timing of ignition, spectral recording, and schlieren imaging was synchronized using a master trigger signal. Schlieren imaging was recorded for the entirety of each experiment, but spectra were recorded only for a short period following a variable delay time, which ensured that emission recording for each condition was not affected by the size of the flame. Spectral recording was delayed until each flame reached a diameter of approximately 10 cm. Flame diameters were verified from the schlieren images.

The spherical flame experimental technique proceeded as follows. First, the vessel was filled to 760.0 torr by the partial pressure method with the appropriate concentrations of methane and air. Fans were used to mix the gases during filling. After mixing, the heaters were turned on and allowed to reach a steady state temperature of 50°C (323 K), which took about 10 minutes. During the heating process, the pressure in the vessel of course increased above the initial filling pressure of 1 atm. This extra gas was vented so that the pressure in the vessel returned to 1 atm. Next, a syringe of 0.75 mL of liquid DMMP was prepared (if required). This liquid volume of DMMP was chosen based on the vapor pressure of DMMP at 50°C and 1 atm (see Table 4 of Ref. [17]) and corresponds to a mole percent of approximately 0.55% in the TFSV at these conditions. The same amount of DMMP was used for each test. The DMMP was added through an injection septum and allowed to evaporate for approximately 5 minutes before

ignition. In the case of the neat CH_4 tests, no DMMP was introduced, and the mixture was ignited after the heating system reached steady state and the excess gas was vented to achieve 1-atm initial pressure.

The general procedure for correcting the raw intensity data into the true spectra data was based on the Princeton Instruments IntelliCal® calibration lamp and the light collection efficiencies of the camera and spectrometer. The efficiencies were obtained from the operation manuals of the devices and then multiplied together to obtain the total, combined system efficiency, which is referred to herein as the "system efficiency". The total system efficiency is less than 10% for the full range of wavelengths (200–800 nm), peaking just below 10% near 300 nm, and generally decreases as wavelength increases, reaching a minimum efficiency of approximately 0.5% at 800 nm. The camera and the spectrometer exhibit peak efficiencies near 400 nm and 300 nm, respectively, and both units lose efficiency gradually as wavelength increases. The system efficiency was used to correct the calibration lamp measurement. First, the calibration lamp output was measured and corrected based on the system efficiency. Then, the calibration lamp reading was compared to the manufacturer's specified calibration curve. It was found that the optical system was slightly under-sensitive near 450 nm, slightly over-sensitive between 525-650 nm, and sufficiently accurate everywhere else. The ratio of the two was computed, providing a scaling factor with which to calibrate the experimental intensity data.

4 Results and Discussion

Figure 1 shows spectra obtained using the 300-lines/mm grating for wavelengths between 200 and 400 nm. This wavelength setting and grating provide a low-resolution view of the OH* features near 310 nm. For the neat CH_4-air flames, Fig. 1a shows that OH* intensity is strongest for $\phi = 1.0$, with its peak intensity being almost a factor of 3 greater than the corresponding emission for $\phi = 0.8$. The intensity of the OH* emission peak for $\phi = 1.2$ lands nearly halfway between the intensities of the other two ϕ. The DMMP-doped flames exhibit a similar trend, as shown in Fig. 1b, with emission for $\phi = 1.0$ outstripping the intensities of either the lean or the rich case. For the doped flames, three repetitions of the stoichiometric case were conducted to show the consistency and repeatability of the experimental procedure, which is confirmed by the strong agreement between the three repeated tests. The addition of DMMP caused emission at $\phi = 1.0$ to increase relative to the neat mixture, but slightly decreased the intensity at these wavelengths for $\phi = 0.8$ and 1.2. A new, weak feature appeared for $\phi = 1.0$ and 1.2 near 325 nm. The OH* peak for the stoichiometric doped flame was stronger than that of the neat flame, but the most significant difference lies in the ~3-fold increase in the broadband emission relative to the neat flame. Although this increase was most apparent in the $\phi = 1.0$ flames for wavelengths longer than 325 nm, there was still a ~50% increase in the broadband emission for the off-stoichiometric cases.

Using the 1200-lines/mm grating, high-resolution spectra were obtained for a 50-nm band focused on the OH* features near 310 nm, which are shown in Fig. 2. This grating reduces line broadening relative to the 300-lines/mm grating. In contrast with Fig. 1, this high-resolution grating allows for the differentiation of the separate emission peaks near 306 nm and 308 nm, which can be seen in both the neat flames (Fig. 2a) and the doped flames (Fig. 2b). The intensity of emission tends to increase by factors of 2-3 when DMMP is added, depending on ϕ, and the new feature near 324 nm can be seen for the stoichiometric flame in Fig 2b. Altogether, the main effect of DMMP addition is to make the emission stronger, albeit noisier, at these wavelengths.

The 1200-lines/mm grating was also used to obtain spectra for wavelengths of 430±25 nm, as presented in Fig. 3, to investigate effects of DMMP addition on CH* emission near 430 nm. The neat flames, shown in Fig. 3a, exhibited differing strengths of CH* emission, with $\phi = 1.2$ presenting the strongest peak. Although $\phi = 1.0$ also has a strong CH* feature, its peak is slightly lower than that of $\phi = 1.2$, while also sustaining a higher level of broadband emission away from the peak. The CH* feature of the lean case is nearly lost in the already low level of broadband emission, which, as expected for a lean flame, indicates little CH* activity. The DMMP-doped flame spectra in Fig. 3b show an increased level of broadband emission that increases as wavelength increases. The stoichiometric flame was strongly

affected by this behavior, much more so than the off-stoichiometric cases, but the increase in broadband emission for $\phi = 0.8$ was enough to cloak its already weak CH* feature.

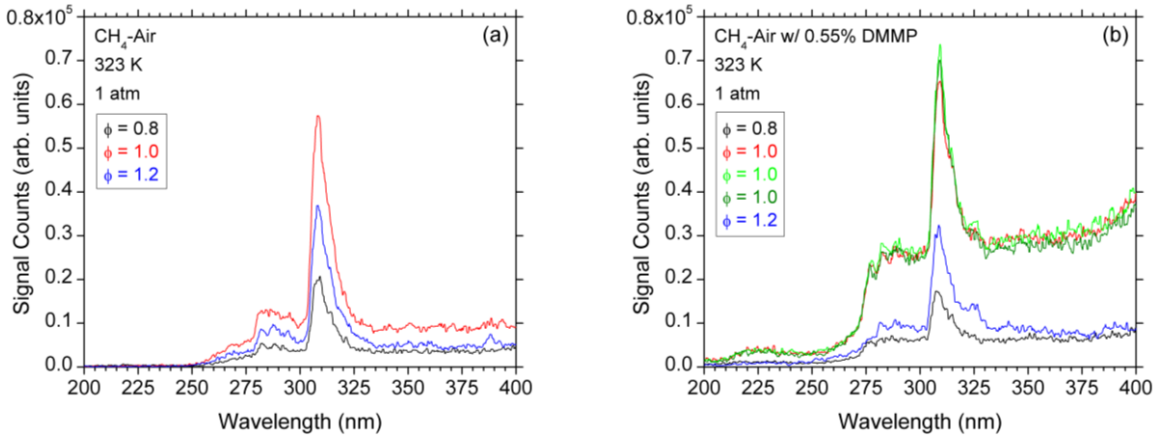

Figure 1: Comparison of low-resolution (300 lines/mm) spectra of (a) neat CH_4-air spherical flames and (b) doped DMMP-CH_4-air spherical flames from 200-400 nm, showing OH* features near 310 nm.

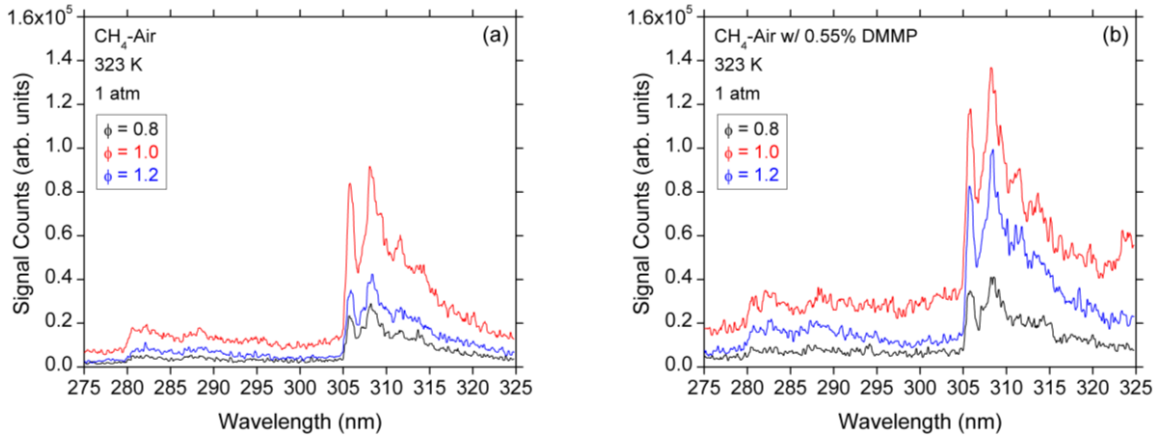

Figure 2: Comparison of high-resolution (1200 lines/mm) spectra of (a) neat CH_4-air (spherical) flames and (b) doped DMMP-CH_4-air flames at 300±25 nm.

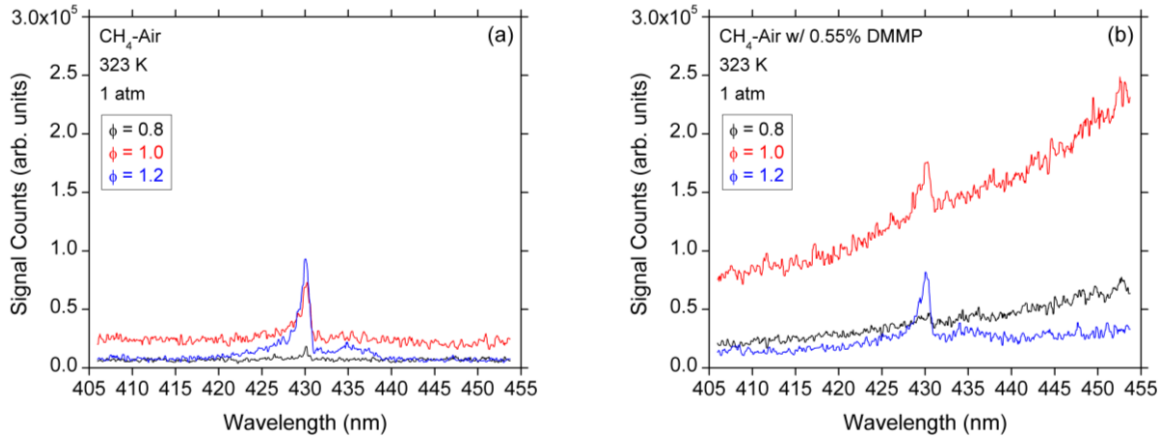

Figure 3: Comparison of high-resolution (1200 lines/mm) spectra of (a) neat CH_4-air (spherical) flames and (b) doped DMMP-CH_4-air flames for 430±25 nm.

The most significant differences between the neat and doped flames can be found in the emission between 400 and 800 nm. Shown in Fig. 4a, the neat CH_4 results show clear CH* features near 430 nm

for all three ϕ, C_2* swan bands near 470 and 515 nm, H_2O emission near 718 nm for ϕ = 1.2, and potential sodium contamination of the stoichiometric flame near 590 nm. In contrast, the DMMP-doped flames exhibit no defining features from 400-800 nm, except faint CH* peaks near 430 nm for ϕ = 1.0 and 1.2. For the neat mixtures, the ϕ = 1.2 flame tends to be slightly more intense than the ϕ = 0.8 flame, but that trend is reversed for the doped mixtures. As shown in Fig. 4b, at longer wavelengths, the intensity of the doped flames is well over one order of magnitude stronger than the neat CH_4 flames. Even at these small mixture fractions, DMMP induces a massive intensity increase that resembles blackbody radiation, although the lean flame shows a decrease in intensity for wavelengths longer than ~675 nm that was observed in multiple repeated experiments. For reference, scaled blackbody spectral distributions are shown in Fig. 4b and were calculated using Planck's law at temperatures that closely match the spectral trends for each ϕ. These blackbody curves were corrected using the optical system calibration, showing that the low optical efficiency causes a drop in intensity at longer wavelengths similar to the spectral measurements. Although these temperatures are lower than the adiabatic flame temperatures predicted by equilibrium chemistry for these mixtures (2174 K, 2176 K, and 2020 K, respectively for ϕ = 0.8, 1.0, and 1.2), the spectra and the blackbody trends show strong qualitative agreement. Deviations between the measured emission and the predicted blackbody emission are likely due to the temperature distribution in the experiment; i.e., the soot in the flame possesses a range of temperatures driven by radiation losses. This hypothesis is supported by the appearance of a gray-brown residue covering the inside of the chamber after DMMP experiments for ϕ = 1.0 and 1.2. This residue clouded the windows and required the chamber to be wiped clean after each DMMP experiment. The residue was not present after neat methane experiments, indicating that the residue consisted of phosphorus-based particles that were likely the source of the intense, broad emission in the doped flames.

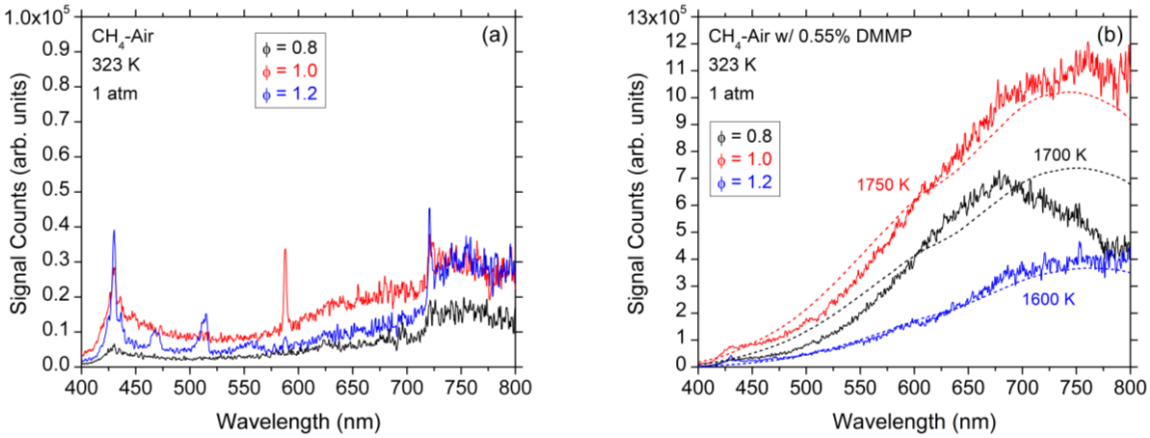

Figure 4: Comparison of low-resolution (300 lines/mm) spectra from 400-800 nm of (a) neat CH_4-air (spherical) flames and (b) doped DMMP-CH_4-air flames with corrected blackbody curves shown. Dashed lines indicate blackbody emission at temperatures listed.

5 Conclusions

Spectra obtained from methane-air flames doped with DMMP show that the addition of DMMP drastically changes the emission spectra of hydrocarbon flames to consist primarily of a broadband continuum. Neat methane-air flames clearly exhibited C_2* Swan bands and OH*, CH*, and H_2O features, depending on the equivalence ratio, but these features were largely overshadowed by the broadband emission in the flames doped with DMMP, although the OH* and CH* peaks near 307 nm and 430 nm, respectively, were still detectable. The rise in emission intensity for intermediate wavelengths imitated blackbody emission, likely from condensed-phase P-based particles, but the efficiency of the optical system caused measured spectra to fall below the blackbody curves for red and near IR wavelengths. When compared to the neat flames, the intensity of the doped flames was over an

order of magnitude higher. The doped-flame spectra otherwise presented no defining features that would implicate an excited P-species like PO_2*. These findings indicate that the primary "feature" of the spectral emission of P-containing flames likely comes from blackbody radiation.

References

[1] Sikes T, Mathieu O, Kulatilaka WD, Mannan MS, and Petersen EL. (2019). Laminar flame speeds of DEMP, DMMP, and TEP added to H_2- and CH_4-air mixtures. Proc. Comb. Inst. 37: 3775.

[2] Mathieu O, Sikes T, Kulatilaka WD, and Petersen EL. (2020). Ignition delay time and laminar flame speed measurements of mixtures containing diisopropyl-methylphosphonate (DIMP). Combust. Flame. 215: 66.

[3] Babushok VI, Linteris GT, Katta VR, and Takahashi F. (2016). Influence of hydrocarbon moiety of DMMP on flame propagation in lean mixtures. Combust. Flame. 171: 168.

[4] Mathieu O, Kulatilaka WD, and Petersen EL. (2018). Experimental and modeling study on the effects of dimethyl methylphosphonate (DMMP) addition on H_2, CH_4, and C_2H_4 ignition. Combust. Flame. 191: 320.

[5] Senyurt EI, Schoenitz M, and Dreizin EL. (2020). Rapid destruction of sarin surrogates by gas phase reactions with focus on diisopropyl methylphosphonate (DIMP). Defence Tech.

[6] Glaude PA, Melius C, Pitz WJ, and Westbrook CK. (2002). Detailed chemical kinetic reaction mechanisms for incineration of organophosphorus and fluoroorganophosphorus compounds. Proc. Comb. Inst. 29: 2469.

[7] Twarowski A. (1993). Photometric determination of the rate of H_2O formation from H and OH in the presence of phosphine combustion products. Combust. Flame. 94: 341.

[8] Twarowski A. (1993). The influence of phosphorus oxides and acids on the rate of H + OH recombination. Combust. Flame. 94: 91.

[9] Twarowski A. (1995). Reduction of a phosphorus oxide and acid reaction set. Combust. Flame. 102: 41.

[10] Davies PB, Thrush BA, and Linnett JW. (1968). The reactions of atomic oxygen with phosphorus and with phosphine. Proc. R. Soc. London, Ser. A. 302: 243.

[11] Verma RD, and McCarthy CF. (1983). A new spectrum of the PO_2 radical. Can. J. Phys. 61: 1149.

[12] Fraser ME, and Stedman DH. (1983). Spectroscopy and mechanism of chemiluminescent reactions between group V hydrides and ozone. J. Chem. Soc., Faraday Trans. 1. 79: 527.

[13] Harris DG, Chou MS, and Cool TA. (1985). Experiments concerning phosphorus chemiluminescence. J. Chem. Phys. 82: 3502.

[14] Hamilton PA, and Murrells TP. (1985). Kinetics and mechanism of the reactions of PH_3 with $O(^3P)$ and $N(^4S)$ atoms. J. Chem. Soc., Faraday Trans. 2. 81: 1531.

[15] Hamilton PA, and Murrells TP. (1986). Mechanism for the chemiluminescence in oxygen-phosphorus system. J. Phys. Chem. 90: 182.

[16] Morones A, Turner MA, Leon VJ, Ruehle K, and Petersen EL. (2019). Validation of a New Turbulent Flame Speed Facility for the Study of Gas Turbine Fuel Blends at Elevated Pressure. ASME Turbo Expo: Power for Land, Sea, and Air. Paper No. GT2019-90394.

[17] Butrow AB, Buchanan JH, and Tevault DE. (2009). Vapor Pressure of Organophosphorus Nerve Agent Simulant Compounds. J. Chem. Eng. Data. 54: 1876.